Does equilibrium or nonequilibrium molecular dynamics correctly simulate thermal transport properties of carbon nanotubes?

I-Ling Chang [1,*] Chia-Shing Li,[1] Guan-Shiung Wang,[1] Chi-Lin Wu,[1] and Chih-Wei Chang [2,†]

[1]*Department of Mechanical Engineering, National Cheng Kung University, Tainan 70101, Taiwan*
[2]*Center for Condensed Matter Sciences and Center of Atomic Initiative for New Materials (AI-MAT),*
National Taiwan University, Taipei 10617, Taiwan

There has been a lot of debate on whether non-Fourier thermal conduction can be observed in quasi-one-dimensional materials such as carbon nanotubes (CNTs) and, additionally, whether the phenomenon can be found by equilibrium or nonequilibrium molecular dynamics (EMD or NEMD) simulations. In fact, so far EMD and NEMD simulations have revealed disparities of thermal transport in CNTs, ranging from purely diffusive behavior, to diffusive-ballistic transition, and to non-Fourier thermal conduction. By carefully examining the roles of interfacial thermal resistances and applied temperature differences in NEMD simulations, we show that the two effects often yield spurious results. After removing the unwanted effects that have been overlooked by previous works, we find that most EMD and NEMD simulations on CNTs consistently display diffusive thermal conduction for length $(L) > 200$ nm. The finding is further supported by the disappearance of nonlocal thermal conduction for $L > 200$ nm. Our results clarify many discrepancies of previous works and point out that nonideal thermostats commonly used in EMD and NEMD simulations would give an effective contact thermal resistance that misleads data interpretations. Overall, we find EMD and NEMD simulations conducted so far disagree with the current experimental results of nondiffusive thermal conduction in CNTs.

I. INTRODUCTION

Heat transfer phenomena in nanoscale materials are known to be characteristically different from their bulk counterparts [1]. Effects such as phonon transmission across interfaces, phonon scatterings at surfaces/boundaries, and phonon confinements all become more significant in nanoscale. Interestingly, dimensionality of materials has been suggested to play an important role in heat transfer as well [2]. The topic has been raised when people find that in one-dimensional (1D) systems, the thermal conductivity (κ) increases with increasing sample length (L) in an anomalous ($\kappa \sim L^{\alpha}$, $\alpha < 1$) manner, deviating from conventional diffusive ($\alpha = 0$) or ballistic ($\alpha = 1$) thermal conduction [3,4]. Moreover, the anomalous effect also suggests that κ would diverge with L without saturation, and the effect is found to be insensitive to disorders [5,6], the presence of a constant temperature gradient [7], or nonlinear phonon interactions [3,4]. Hence, after the theoretical discovery, the criteria of Fourier's law, the universality of the anomaly, and the underlying physical mechanisms have become long-time puzzles for decades [4,8,9]. Because the heat transfer process in 1D systems apparently deviates from the normal diffusion process, phenomena displaying $\alpha > 0$ are sometimes referred to as non-Fourier thermal conduction [3,4].

Despite the intense theoretical investigations on many 1D toy models, it is curious whether the phenomena could be observed in real materials. Because of the pronounced phonon confinement effect, single-wall carbon nanotubes (CNTs) have been suggested to be quasi-1D systems that may display non-Fourier thermal conduction. However, so far both equilibrium and nonequilibrium molecular dynamics (EMD and NEMD) simulations on CNTs have yielded inconsistent results [10–22]. For example, while some works have suggested that κ would continue to diverge with L without saturation at 300 K, the fitted α's have varied from one to another, even when the simulated CNTs are of identical structures [10,11,14,15,17,19,22]. On the other hand, several works have instead shown that CNTs display ballistic to diffusive transition when L is large, and estimated the phonon mean free path to be ~ 1 μm at 300 K [12,20,21]. Finally, some other works have also reported κ's of CNTs to be length independent, displaying purely diffusive thermal conduction [16,18].

The disagreements between MD simulations have raised concerns. Lukes and Zhong discussed the discrepancies between EMD and NEMD simulations on the value of κ's and attributed them to the length dependence of κ, an effect that was not appreciated at that time [17]. However, they also noted that many discrepancies could not be completely resolved without knowing the subtleties in the MD simulations, such as interatomic potentials, boundary conditions, and thermal baths, etc. [17]. There were also discrepancies between MD simulations and results from the Boltzmann transport equation [16,23,24]. For example, Mingo and Broido incorporated three-phonon scattering processes and found that the

————
*ilchang@mail.ncku.edu.tw
†cwchang137@ntu.edu.tw

divergence of κ would terminate at $L \sim 1$ mm [23]. On the other hand, Donadio and Galli compared EMD simulations and Boltzmann transport equations and found that κ would saturate at ~ 7000 W/mK when $L \sim 20$ nm [16]. Recently, Sääskilahti *et al.* pointed out higher-order scatterings were either neglected or treated approximately in previous calculations [22]. They instead extrapolated phonon mean free paths from their NEMD simulation to follow $\omega^{-0.97}$ (ω is phonon frequency) for low-frequency phonons and suggested κ would continue to increase at least up to $L = 4\,\mu$m [22].

Experimentally, length-dependent κ measurements have been conducted by several groups. Chiu *et al.* studied length-dependent thermal transport by using electrical breakdown of multiwall CNTs and estimated the phonon mean free path to be 0.2 μm [25]. Chang *et al.* simultaneously measured length-dependent electrical and thermal transport of multiwall CNTs and demonstrated that the κ vs L relation deviated from the electrical, diffusive counterparts for $L \sim 4\,\mu$m [26]. They found $\alpha = 0.6$ to 0.8, closer to conventional ballistic thermal conduction. Liu *et al.* employed optical measurement to probe the κ vs L relation of a single-wall CNT [27]. They found $\kappa \sim L^{0.65}$ up to $L = 5\,\mu$m and then κ saturated at $L > 10$ μm. However, the latter claim was inconclusive due to the intrinsic noise associated with their optical measurements. Recently, Lee *et al.* improved the measurement sensitivities and obtained the length dependence of κ for $L > 1$ mm [28]. Interestingly, they found $\alpha = 0.2$ to 0.5 for $L > 400$ μm, falling within the α's estimated from 1D models [2]. From these works, we found strong experimental evidence for room temperature non-Fourier thermal conduction, at least at microscale.

Because a genuine non-Fourier thermal conductor would display $\kappa \sim L^{\alpha}$, many researchers plotted κ vs L data and interpreted the divergence of κ as the evidence of non-Fourier thermal conduction. On the other hand, because of the mismatch of the phonon spectrum between thermal baths and the sample, interfacial thermal resistances would occur at the boundaries of an investigated system. Recently, we pointed out that finite interfacial thermal resistance would give spurious divergence of κ, leading to misinterpreting the experimental data as evidence of ballistic thermal conduction in Si or Ge [29].

To emphasize our point, we note that the κ vs L relation reflects the thermal transport of the whole investigated system, which includes the sample and the contacts jointing the thermal baths. The statement is correct for any experimental measurements as well as any NEMD simulations that employ thermal baths. Thus, for a thermal conductor (assuming $\kappa_{\text{sample}} \sim L^{\alpha}$, or equivalently, $R_{\text{sample}} = aL^{1-\alpha}$, where a is a constant) jointing to two thermal baths, the total thermal resistance (R_{total}) of the system can be expressed as

$$\text{R}_{\text{total}} = aL^{1-\alpha} + R_c, \tag{1}$$

where R_c is the interfacial thermal resistance. Following the definition $\kappa \equiv L/RA$ (where A is the cross-sectional area of the sample), we can convert R_{total} into total thermal conductivity of the investigated system (κ_{total}):

$$\kappa_{\text{total}} = \frac{L/A}{aL^{1-\alpha} + R_c}. \tag{2}$$

We note that $\kappa_{\text{total}} \to 0$ as $L \to 0$ even for $\alpha = 0$ (i.e., diffusive thermal conduction). Thus if we simply plot the κ_{total} vs L data without noticing the presence of R_c in the system, one could misinterpret the data as the evidence for non-Fourier thermal conduction. As shown in Fig. 1(a), the κ_{total} vs L relation of a diffusive conductor with finite R_c would look very similar to that of a non-Fourier thermal conductor with $\alpha = 0.206$. Furthermore, a non-Fourier thermal conductor for $\alpha = 0.3$ and finite R_c could be mistakenly regarded as for $\alpha = 0.51$ with $R_c = 0$. Although one may investigate samples of very long lengths [i.e., $L \gg \sqrt{R_c/a}$, as displayed by $L > 12$ in Fig. 1(a)] to make a distinction, the criterion usually goes beyond the capabilities of ordinary MD simulations and cannot be realized in practice.

Because $R_c = 0$ should not be *a priori* in any investigated systems, we have advocated to plot the AR_{total} vs L relation ($AR_{\text{total}} \equiv L/\kappa_{\text{total}}$) to avoid data misinterpretation [29]. Accordingly, the contribution of R_c's can be read from the intercept at the y axis when $L \to 0$, as shown in Fig. 1(b). After removing the unwanted R_c, the method will help to uncover the unambiguous evidence for non-Fourier thermal conduction, as displayed in Fig. 1(c).

In addition, we note that the above phenomena are established on the theorem of linear responses; that is, non-Fourier thermal conduction should not vanish when the applied temperature difference (ΔT) across the sample is reduced. In practice, ΔT is always kept large (>20 K) in most NEMD simulations to minimize uncertainties caused by thermal fluctuation. One is thus required to justify the ΔT used in the simulation and demonstrate that the non-Fourier thermal conduction is robust when the ΔT becomes smaller.

In this paper, we investigate the effects of R_c and ΔT to thermal transport of CNTs using NEMD simulations. In Sec. II, we discuss the simulation method. In Sec. III, we show that even when a linear temperature profile of a CNT is used for estimating κ's, unwanted effects of R_c still emerge in the κ vs L relation, yielding spurious non-Fourier thermal conduction. We have confirmed our finding by changing the mass of thermal baths to induce R_c. Furthermore, we also find that reducing ΔT would make the non-Fourier thermal conduction disappear, rendering the estimated α's unreliable. In Sec. IV, we reexamine previous works and find that the overlooked effects could invalidate previous findings on non-Fourier thermal conduction or ballistic-diffusive transitions. In fact, most EMD and NEMD simulations consistently give diffusive thermal transport starting at very short L's. However, they disagree with experimental results. In Sec. V, additional support based on nonlocal thermal conduction is shown to give consistent results that CNTs behave like a diffusive thermal conductor for $L > 200$ nm. In Sec. VI, we discuss the idea that the origin of the R_c could be due to nonzero output thermal resistance from a nonideal thermostat. Finally, we summarize the results and discuss some possible directions to remedy the problems.

II. METHODS

The nonequilibrium molecular dynamics approach was employed to study thermal conductivity of (4,4) nanotubes using the LAMMPS package. Here a temperature difference
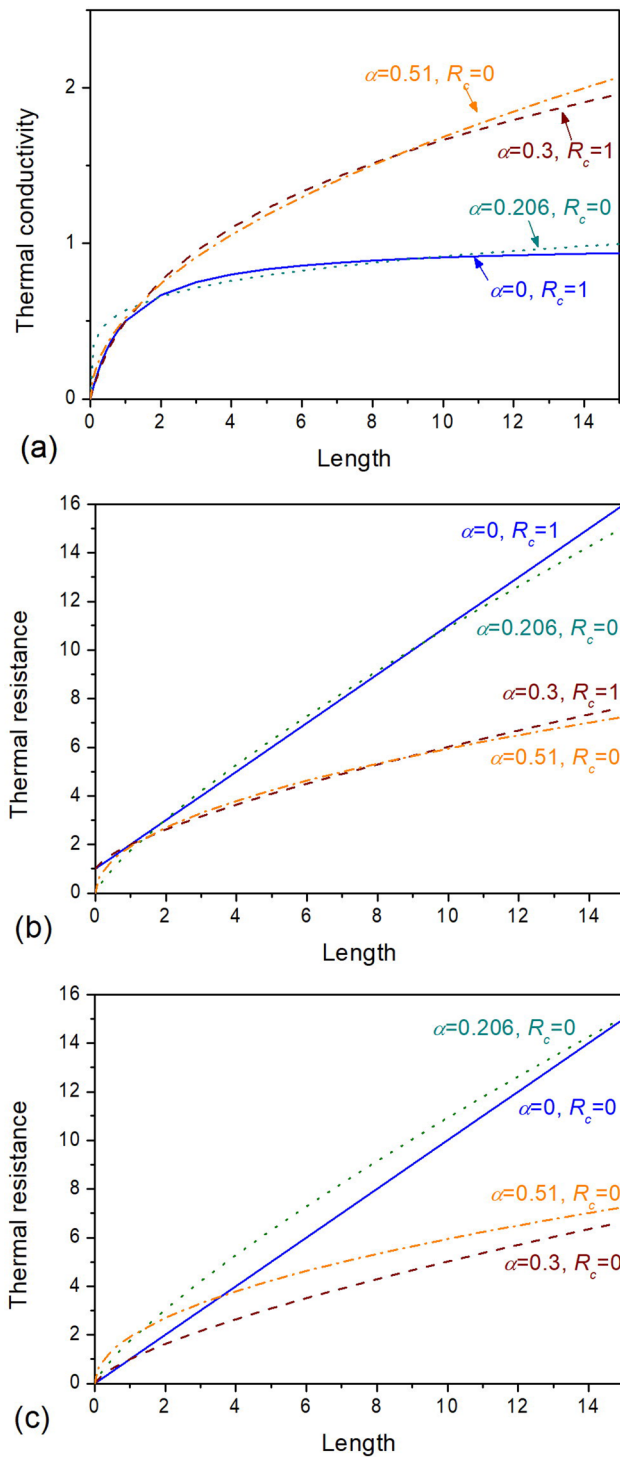
(a)

FIG. 1. (a) κ vs L relation of a diffusive conductor ($\alpha = 0$, blue solid line) with $R_c = 1$ would look very similar to that of a non-Fourier thermal conductor with $\alpha = 0.206$ and $R_c = 0$ (dark cyan dotted curve). Additionally, a non-Fourier thermal conductor with $\alpha = 0.3$ and $R_c = 1$ (brown dashed curve) could be mistakenly regarded as $\alpha = 0.51$ with $R_c = 0$ (orange dashed-dotted curve). Here we have assumed $\kappa = L^{\alpha}$. (b) When plotting the corresponding data using R_{total} vs L, the contribution of R_c's can be estimated by the intercept at the y axis when $L \to 0$. (c) After removing the unwanted contribution of R_c's, the data can reveal non-Fourier thermal conduction. Here the thermal conductivity, thermal resistance, and lengths are of arbitrary units.
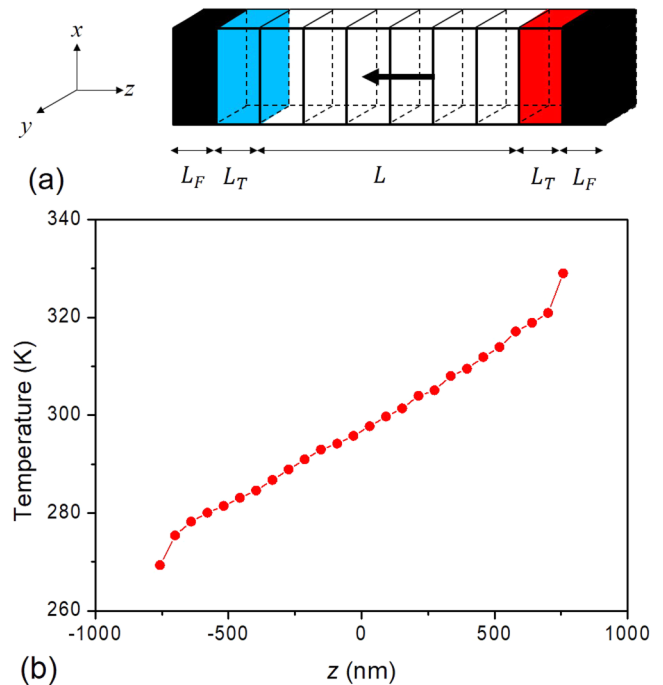

FIG. 2. (a) A CNT in a nonequilibrium MD simulation is divided into a number of equal cells. Fixed boundary conditions are applied at two ends next to the thermal controlled region. (b) A representative temperature profile of a 1.5-μm-long CNT. To minimize the unwanted effects of interfacial thermal resistance that appear as the apparent temperature jumps at the ends of the CNT, we have focused our analysis to the central region ($z = -375$ to 375 nm here), where a linear temperature gradient can be observed, to determine the system's κ_{total}.

ΔT was imposed through two temperature controlled regions (20 unit cells each, 320 atoms in one unit cell). Next to the temperature controlled regions, the atoms at the two ends (two unit cells) were fixed as shown in Fig. 2(a). The temperature control was achieved through a Langevin thermal bath. Using second-generation reactive empirical bond order (REBO) potential and fixed boundary conditions, we employed the velocity Verlet method to integrate the equation of motion with a time step of 0.5 fs. First, the entire nanotube was coupled to a Nosé-Hoover thermostat at 300 K and MD was performed to equilibrate and relax the system for 1 ns. After equilibrium, the hot (cold) bath temperature was set to $T + \Delta T / 2 (T - \Delta T / 2)$, respectively, and ran for 2 ns under a microcanonical ensemble. In our simulations, we took $\Delta T = 20$, 40, and 60 K to examine the effect of temperature difference. The heat flux P was computed from the energy in/out of the temperature controlled regions. The simulated nanotube was divided into several equal cells and the temperature at each cell was calculated and averaged for 1 ns after reaching steady state.

Figure 2(b) shows a representative temperature profile of (4,4) CNT at $\Delta T = 40$ K. There are apparent temperature jumps at the ends of the CNT, indicating finite interfacial thermal resistance between the CNT and the thermal baths. To remove the obvious unwanted effect, we have focused on the linear region at the middle ($z = -L/4$ to $L/4$) to analyze

the thermal conductivity of the investigated system (κ_{total}), following

$$\kappa_{\text{total}} = \frac{P}{A(dT/dz)}, \tag{3}$$

where P is the heat flux and the CNT cross section $A = \pi D \delta$ (D is the diameter of the CNT, $\delta = 0.34$ nm). As will be shown below, we will find that κ_{total} is not the intrinsic thermal conductivity of the CNT even if we have focused our analyses on the linear temperature profile region far away from the interfaces.

The T-junction and cross-junction CNTs in Sec. V, were created by a thermal welding method as proposed in the literature [30], where some atoms were removed manually from one pristine (6,6) nanotube of 4 nm to create defects in the crossing region. Then another 1.5 nm (6,6) CNT was placed vertically above the crossing region of the defected CNT. Then, these two nanotubes were moved closer and simultaneously heated up to 4000 K for 2 ps to perform thermal welding before they were cooled down to 300 K. The branched CNT was created by connecting three (6,6) nanotubes of the same lengths to the junction part. To release the stress inside the branched CNT, the atoms on each individual branch were only allowed to move along its axial direction under *NVE* ensemble and the equilibrating process was run for 1 ns. Through this relaxation procedure, both longitudinal and transverse stresses inside the branches were eliminated.

III. LENGTH-DEPENDENT THERMAL CONDUCTIVITY AND THERMAL RESISTANCE

Figure 3(a) shows κ_{total} vs L relations for the mass of the thermal bath respectively assigned to be $m_T = 6$ and 18 (where m_T is the atomic mass of the thermal bath, and $m_T = 12$ for carbon atoms). For comparison, we also plot κ_{total} vs L relations without removing the temperature jumps shown in Fig. 2(b). At first sight, all the κ_{total}'s apparently increase with increasing L and deviate from diffusive behavior (i.e., $\kappa_{\text{total}} = $ constant). A naïve fitting to the κ_{total} vs L relations shown in Fig. 3(a) indicates non-Fourier thermal conduction with $\alpha = 0.26$ and 0.44 for $m_T = 6$ and 18, respectively. However, as we have emphasized earlier, interpreting the data based on the κ_{total} vs L relation could be misleading and plotting the AR_{total} vs L relation is more reliable. Indeed, after plotting the AR_{total} vs L data in Fig. 3(b), we find that all data have a nonzero intercept at $L \to 0$, indicating finite interfacial thermal resistance. A simple calculation on the phonon reflectivity suggests that R_c for $m_T = 6$ is 1.6 times larger than that of $m_T = 18$, which quantitatively agrees with the results read from the simulated temperature jumps. From the intercept at $L \to 0$ shown in Fig. 3(b), we find that the interfacial thermal resistance is about two times higher for data including temperature jumps than that excluding temperature jumps. Because the latter is nonzero, it suggests that a residue R_c still contributes to the investigated system even when we have excluded the apparent temperature jumps in CNT's temperature profiles. Importantly, now the AR_{total} vs L relation shown in Fig. 3(b) is almost linear for $m_T = 18$, suggesting diffusive thermal conduction. Thus the spurious non-Fourier thermal conduction for $m_T = 18$ shown in Fig. 3(a) is in fact
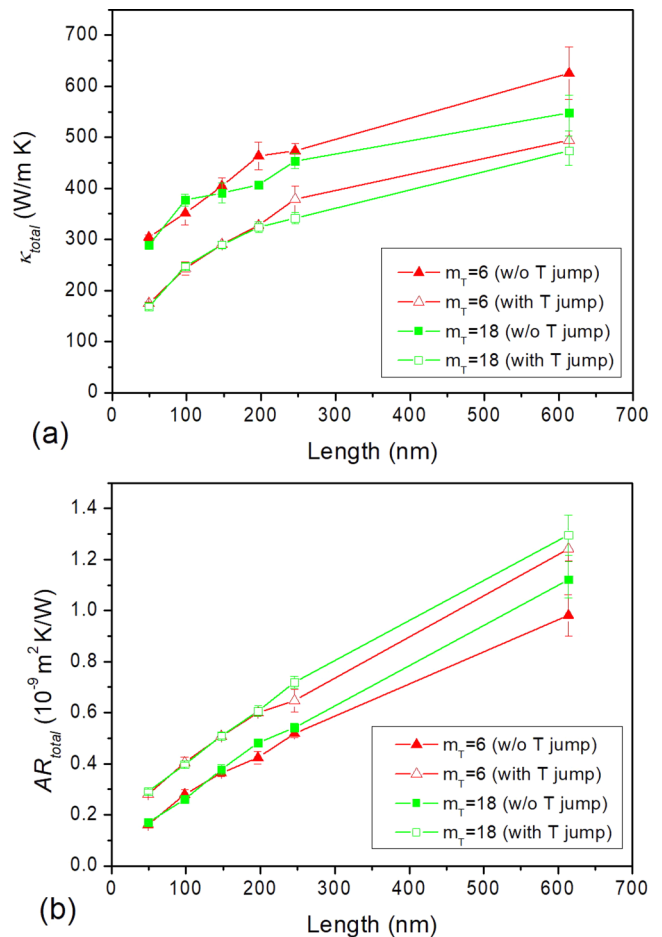

FIG. 3. (a) κ_{total} vs L of a (4,4) CNT simulated using thermal baths of different atomic mass ($m_T = 6$ and 18). The solid symbols are obtained after removing temperature jumps shown in Fig. 2(b). We also plot the results containing the temperature jumps for comparison (open symbols). At first sight, all the curves appear to indicate non-Fourier thermal conduction with $\alpha = 0.26$ to 0.44. (b) The corresponding data plotted in AR_{total} vs L relation, but now the curves do not significantly deviate from diffusive transport and $\alpha = 0$ to 0.1 is found. We also find that all the data have nonzero intercept at $L \to 0$, indicating finite interfacial thermal resistance. Note that, for the data without incorporating temperature jumps, their interfacial thermal resistance ($AR_c = 0.09 \times 10^{-9} \, \text{m}^2 \, \text{K/W}$) still contributes about half of that containing temperature jumps. It indicates that the removal of the temperature jumps is not sufficient to completely eliminate the interfacial thermal resistance of the system.

an artifact due to the finite R_c. For $m_T = 6$, the AR_{total} vs L curve slightly deviates from diffusive behavior and $\alpha = 0.05$ to 0.1 is found. But, as will be discussed later, we will find the data of $m_T = 6$ to be due to another spurious effect from ΔT.

To minimize the unwanted effect of interfacial thermal resistances, we note that minimum R_c is expected when assigning $m_T = 12$. On the other hand, we note that the features of non-Fourier thermal conduction should follow the linear response theorem; that is, the features should not disappear when ΔT is reduced. To investigate the robustness of the feature, we have simulated CNTs with $m_T = 12$ under $\Delta T = 60$, 40, and 20K, respectively. Figures 4(a) and 4(b) show that,
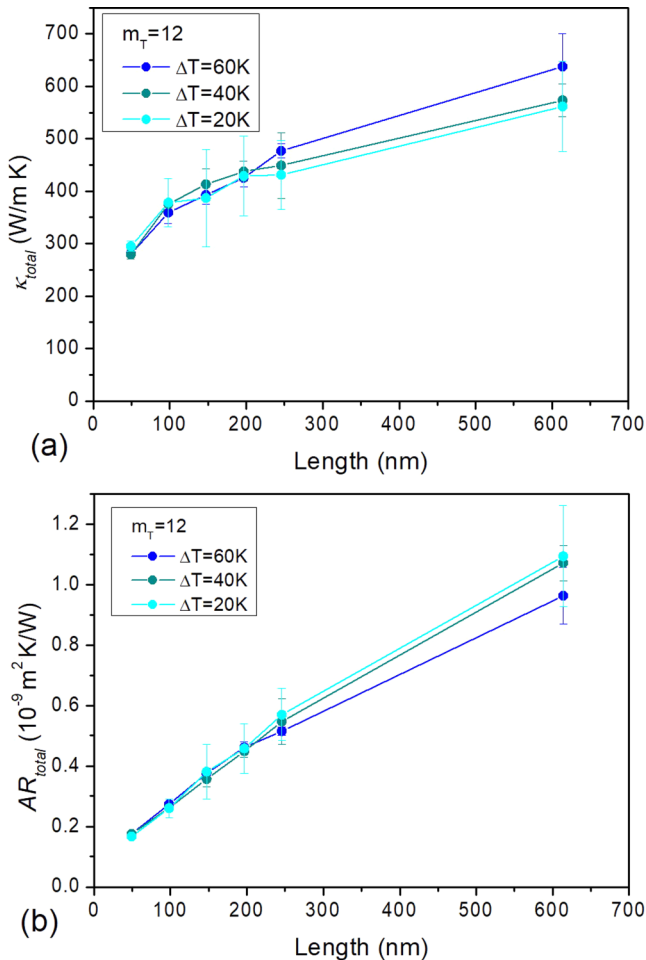
FIG. 4. (a) κ_{total} vs L of a (4,4) CNT under $\Delta T = 60$, 40, and 20 K, respectively. Here the atomic mass of the thermal bath is $m_T = 12$. (b) Corresponding data displayed using AR_{total} vs L. Although the data of $\Delta T = 60$ K display features like non-Fourier thermal conduction with $\alpha = 0.08$, the thermal transport becomes almost diffusive ($\alpha < 0.02$) when $\Delta T = 40$ and 20 K. The inconsistency thus excludes the data at $\Delta T = 60$ K to be genuine features of non-Fourier thermal conduction.

although the κ_{total} vs L and AR_{total} vs L relations under $\Delta T = 60$ K display features such as non-Fourier thermal conduction (finite R_c is still found here) with $\alpha = 0.08$, the thermal transport becomes almost diffusive ($\alpha < 0.02$) for $\Delta T = 40$ and 20 K, respectively. The inconsistency thus excludes the data of $\Delta T = 60$ K to be genuine features of non-Fourier thermal conduction. Instead, unwanted nonlinear thermal responses are more likely to be responsible for the observed phenomena. Therefore, after removing the unwanted effects of R_c and ΔT, so far our NEMD simulations have consistently displayed diffusive thermal conduction in (4,4) CNTs.

IV. REEXAMINATION OF PREVIOUS RESULTS

Having clarified the effects that could mislead the data interpretation, we now reexamine previous results based on MD simulations. Table I summarizes the information we collected from previous works, which includes EMD and

NEMD simulations, CNT of different chiralities, interacting potentials, boundary conditions, thermal thermostats, etc. Because of their differences, it may not be surprising that the claims also vary from one to another.

Almost all previous works have interpreted their data based on κ vs L relations [10–22], but as we have mentioned above, the analysis can be problematic and plotting the AR_{sample} vs L after removing the unwanted R_c is more appropriate. We have thus replotted their data into AR_{total} vs L and read AR_c from the intercept when $L \to 0$ regardless of whether the authors of the papers have excluded temperature jumps in their simulations. We then obtain $AR_{\text{sample}} = A(R_{\text{total}} - R_c) = bL^{1-\alpha}$ (here b is a constant, fitted from AR_{sample} at the short L's of each paper), which is the intrinsic thermal resistance of the CNT. Because the b's also vary from one to another, we have further normalized them and plotted AR_{sample}/b vs L in Fig. 5(a) to highlight their length-dependent behavior. An enlarged view for $L < 300$ nm is shown in Fig. 5(b).

Many works have claimed to observe anomalous thermal conduction in CNTs with $\alpha = 0.1$ to 0.36. However, we find only Zhang and Li's (10,10) CNT [15], Shiomi's (3,3) CNTs [19], and Sevik et al.'s (10,0) CNT [21] display observable deviation from diffusive thermal conduction, as shown in Figs. 5(a) and 5(b). Even so, the reanalyzed α's are smaller than previous claims, falling within $\alpha < 0.1$. They could be indistinguishable from diffusive behavior after further incorporating simulation errors.

Some other previous works have observed ballistic to diffusive transition when L increases [12,20,21]. The characteristic length associated with the transition has been interpreted as the phonon mean free path of CNTs. However, the claim is not supported after our reanalyses. As displayed in Figs. 5(a) and 5(b), most of the works show diffusive transport starting at $L < 50$ nm. These results contradict experimental observation that non-Fourier thermal conduction of CNTs exceeds 4 μm [26–28].

On the other hand, some EMD simulations have instead suggested diffusive thermal transport in CNTs [16,18]. We find the claim is sustained after our reanalyses. We also find $R_c = 0$ in our reanalysis, which is expected as no thermostat is employed in EMD simulations. The results clearly show that the diffusive thermal transport in CNTs and the presence of finite R_c has different origins. However, as mentioned above, the claim disagrees with experimental results.

Because thermal transport properties of a large-diameter CNT are expected to be similar to those of graphene, the same phenomena will be likely to be observed whenever MD simulations are employed in graphene as well. In addition, if diffusive thermal conduction in CNTs of small diameter appears at much shorter L's than previously thought, it would imply MD simulations would always give a very short phonon mean free path in graphene as well. Indeed, the NEMD simulation on graphene display a nearly diffusive result for $L > 30$ nm after we replot the data of Refs. [20,31,32] into AR_{total} vs L. The misinterpetation is again due to the overlooked R_c in the NEMD simulation. In addition, the diffusive transport is consistent with that obtained from EMD simulations [33,34]. Thus our reanalysis further highlights that the empirical interatomic potential of sp^2 bonds would

TABLE I. Summary of previous publications. Here the α's denoted by * are fitted from the published κ vs L relation.

| Publication	CNT index	α Reported	$AR_c(10^{-9}\,\mathrm{m^2\,K\,W^{-1}})$	ΔT	Potential
Maruyama [10]	(5,5)	0.32	0.038	20 K	TB
Maruyama [11]	(5,5)	0.27	0.036	20 K	Simplified Brenner
	(8,8)	0.15	0.02		
	(10,10)	0.11	0.008		
Moreland et al. [12]	(10,10)	Ballistic-diffusive	0.183	20 K	TB
Padgett and Brenner [13]	(10,10)	0.67*	0.302	?	REBO
Zhang and Li [15]	(5,5)	0.4	0.003	20 K	Tersoff
	(10,10)	0.36	0.003		
Lukes and Zhong [17]	(10,10)	0.94*	0.24?	N/A	(EMD) REBO
	(10,10)	0.8*	0.158		
Donadio and Gallo [16]	(10,0)	0	0	N/A	(EMD) Tersoff
Shiomi and Maruyama [19]	(3,3)	0.4*	0.058	20 K	Simplified Brenner
	(5,5)	0.28*	0.034		
Bi et al. [18]	(15,0)	0*	0	20 K	Tersoff
	(10,10)	0*	0		
Thomas et al. [20]	(6,6)	Ballistic-diffusive	0.4	>12 K (depending on length)	REBO
	(8,8)		0.24		
	(10,10)		0.41		
Sevik et al. [21]	(10,0)	Ballistic-diffusive	0.116	60 K	Tersoff
	(10,10)		0.11		
Sääskilahti et al. [22]	(10,10)	0.38*	0.163	60–200 K	Tersoff
This work	(4,4)	0	0.09	20–60 K	REBO
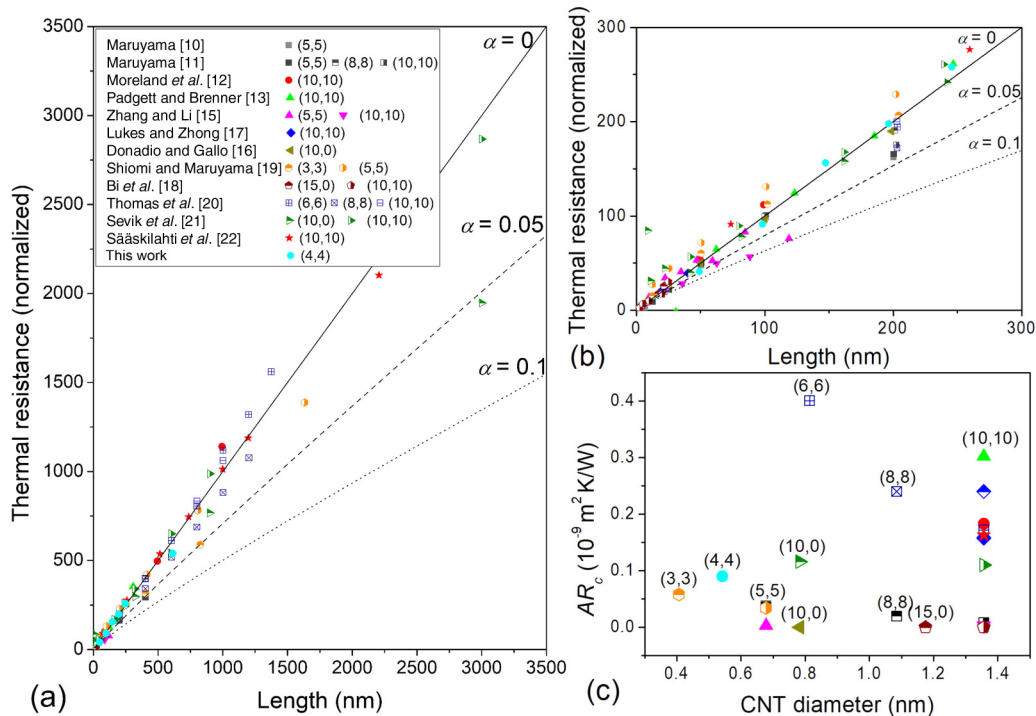
FIG. 5. (a) Normalized thermal resistance vs L summarized from previous works and this work. (b) An enlarged view of (a). It can be seen that most data display nearly diffusive thermal transport (solid line) starting at $L < 200$ nm. Even for a few cases that show indication of non-Fourier thermal conduction, their deviation is found to be small ($\alpha < 0.1$). (c) Summary of AR_c vs CNT diameters estimated from previous works. It can be seen that AR_c varies even when the simulated CNTs are of identical chirality.

consistently yield diffusive thermal conduction in CNTs and graphene.

Regarding ΔT's applied to the simulated systems, we find that many previous works have kept $\Delta T = 20$ K, but there are concerns whether the finding remains robust when ΔT is reduced. On the other hand, some previous works have instead used a constant temperature gradient. For example, Sääskilahti *et al.* have applied $\Delta T = 200$ K to a $L = 4 \, \mu$m CNT and observed non-Fourier thermal conduction [22], but $\alpha < 0.1$ is found after our reanalyses. Thomas *et al.* have applied a temperature gradient 25–80 K/μm ($\Delta T < 57$ K) to their CNTs [20] and found ballistic to diffusive transition at $L = 400$–800 nm, but we could only find diffusive transport throughout their investigated L's after our reanalyses.

V. NONLOCAL THERMAL CONDUCTION

Having learned the overlooked effect of R_c and overestimated α's omnipresent in earlier works, we now seek additional evidence to support our finding. Because R_c arises even when apparent temperature jumps in CNTs have been removed for our analysis, we desire an independent NEMD simulation that can be free from the unwanted effect of R_c.

According to the Landauer-Büttiker formula [35,36], a one-dimensional ballistic electrical conductor connected with multiple terminals will lead to nonlocal electrical conduction, following

$$I_i = G_Q \sum_j (t_{ji} V_i - t_{ij} V_j), \tag{4}$$

where is I_i electrical current flowing out of the *i*th terminal, V_i is electrical voltage on the *i*th terminal, t_{ij} is the transmission probability from the *i*th to the *j*th terminal, and $G_Q = e^2/h$.

The analogy between electrical transport and thermal transport also gives the Landauer-Büttiker formula for nonlocal thermal conduction, i.e.,

$$P_i = K_Q \sum_j (t_{ji} T_i - t_{ij} T_j), \tag{5}$$

where I_i is replaced by the thermal current P_i, V_i is replaced by temperature T_i, and K_Q is quantum thermal conductance obeying Landauer's formalism. Note that Eq. (5) is much simpler than the general formalism of nonlocal thermal conduction in three dimensions and thus will be easier for analysis [37,38]. Besides, in a time reversal-invariant system, $t_{ij} = t_{ji}$ and Eq. (5) can be simplified to

$$P_i = K_Q \sum_j t_{ij} \Delta T_{ij}. \tag{6}$$

Because nonlocal thermal conduction is absent in a diffusive thermal conductor, its presence would infer nondiffusive thermal transport and the effect will be independent of the unwanted effect of R_c.

To investigate nonlocal thermal conduction using NEMD, we arrange a (6,6) CNT of length $2L + L_{th}$ connected to three thermostats with temperatures respectively set at $T_1 = 300$ K, $T_2 = 340$ K, and $T_3 = 320$ K, as shown in Fig. 6(a). Here the thermostat at the middle has length L_{th} but only encompasses a half circumference of the CNT so that phonons leaving from T_3 could propagate across it to reach T_1, which would
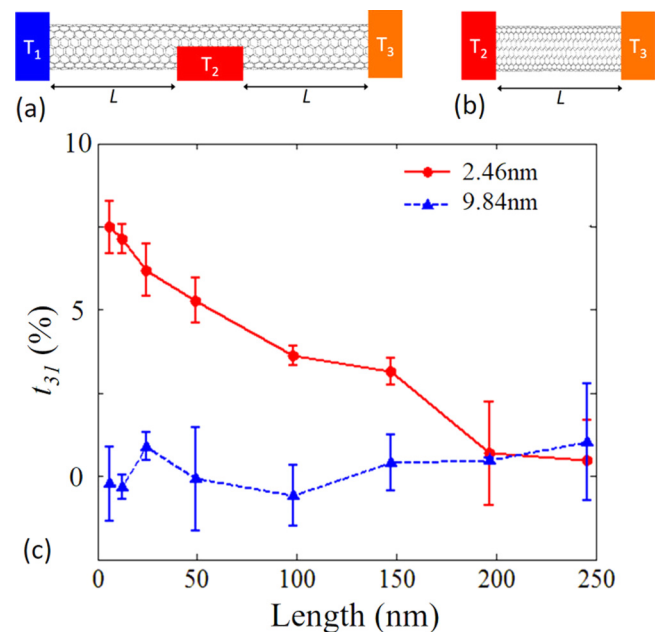

FIG. 6. (a) A (6,6) CNT connected to three independent thermostats for investigating nonlocal thermal conduction. Here $T_1 = 300$ K, $T_2 = 340$ K, and $T_3 = 320$ K. To determine t_{31}, the heat current between T_2 and T_3 is compared with that of a controlled simulation shown in (b). (c) t_{31} vs L for the middle thermostat of lengths $L_{th} = 9.84$ nm (blue triangles) and $L_{th} = 2.46$ nm (red circles), respectively.

contribute nonlocal thermal conduction t_{31}. For a controlled simulation, we have investigated the thermal current of a CNT of length L under identical temperature configurations, as displayed in Fig. 6(b). Because $T_3 - T_1 = T_2 - T_3$, the t_{31} can be obtained from comparing the net thermal current received at terminal 3 in Fig. 6(a) [$P_3 = K_Q t_{31}(T_3 - T_1) + K_Q t_{32}(T_3 - T_2)$, here $t_{31} + t_{32} = 1$], and in Fig. 6(b) [$P'_3 = K_Q(T_3 - T_2)$] via the relation $2t_{31} = 1 - P_3/P'_3$. This method helps us to minimize temperature- or length-dependent effects when determining t_{31}. We have also varied the length (L_{th}) of the middle thermostat and the length (L) of CNT to investigate its effect on t_{31}. Finally, we have confirmed that $t_{31} = 0$ for a purely diffusive thermal conductor of identical geometry, which excludes any nonzero t_{31} observed to be attributed to dimensional effects.

Figure 6(c) displays the t_{31} vs L of a CNT with two different L_{th}'s. Notably, t_{31} remains zero for $L_{th} = 9.84$ nm, indicating that the dissipation of the middle thermostat has completely destroyed nondiffusive properties of low-frequency phonons in the CNT. On the other hand, for $L_{th} = 2.46$ nm, t_{31} reaches 7% for the shortest CNT and gradually decrease to zero when L increases beyond 200 nm, which suggests that the phonon mean free path of the CNT is shorter than 200 nm. Although one may speculate that further reducing L_{th} would elongate the length of nonlocal thermal conduction, extrapolating the data to $L_{th} \rightarrow 0$ indicates that the mean free path remains in the range of 200 nm.

Because the result of Fig. 6(c) is obtained without incorporating unwanted effects of R_c, it is an independent proof that a CNT would be a diffusive thermal conductor when $L > 200$ nm.
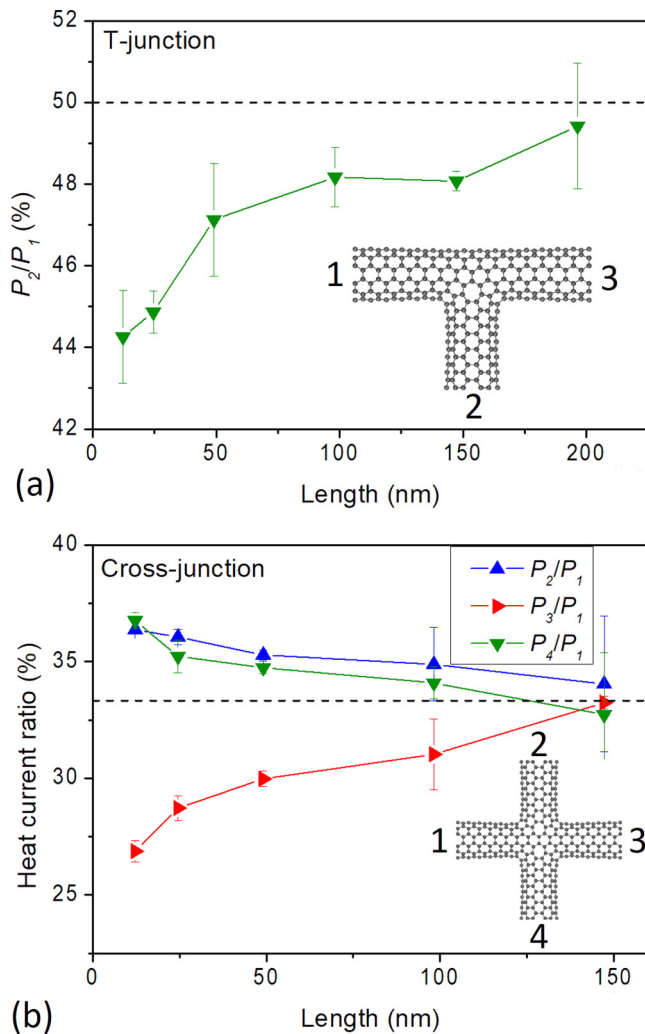
FIG. 7. P_i/P_1 vs L_i for a T junction (a) and a cross junction (b) whose structures are respectively shown in the insets. The predictions of diffusive transport are shown by dashed lines.

The evidence of nonlocal thermal conduction can be further solidified using other systems. As shown in the inset of Fig. 7(a), we now devise a T junction made by three (6,6) CNTs of equal lengths ($L_1 = L_2 = L_3$). We then study how the two branches distribute the heat flow and find their deviations from diffusive thermal conduction when L_i increases. If the system is a diffusive conductor and $T_1 = 330$ K, $T_2 = T_3 = 270$ K, it can be expected that the heat current evenly distributes to each segment. The result still holds when exchanging the temperature settings to $T_2 = 330$ K, $T_1 = T_3 = 270$ K.

Figure 7(a) shows the ratio of total heat current (P_2/P_1) received by terminal 2 when $T_1 = 330$ K and $T_2 = T_3 = 270$ K. It can be seen that $P_2/P_1 = 0.5$ happens only for $L_i > 200$ nm, whereas the unexpected $P_2/P_1 < 0.5$ occurs for $L_i < 200$ nm. In addition, the result seems to indicate that phonons prefer to move forward rather than be scattered by 90°.

However, the results are different in a cross junction made by (6,6) CNTs of equal lengths ($L_1 = L_2 = L_3 = L_4$) shown in the inset of Fig. 7(b). Here the expected diffusive results ($P_2/P_1 = P_3/P_1 = P_4/P_1 = 0.33$) can be found only for $L_i > 150$ nm. Unlike the result from the T junction, here we have

P_2/P_1 to $P_4/P_1 < 0.33$ for $L_i < 150$ nm, which seems to indicate that phonons prefer to be scattered by 90° instead of moving forward.

Because the joints in Figs. 7(a) and 7(b) have identical septagon carbon and octagon carbon rings, the preferred scattering direction should be identical for both cases even if the joint renders some anisotropic phonon scatterings. Thus the results in the T junction and the cross junction being difficult to understand within the picture of diffusive transport. Thus, both the deviation of P_2/P_1 from diffusive transport and the dissimilar anisotropic scatterings must be analyzed using the Landauer-Büttiker formula shown in Eq. (6).

For the cases shown in Figs. 7(a) and 7(b), because of the structural asymmetries induced by the joint and in general $t_{12} \neq t_{13}$, deviations from $t_{12}/(t_{12} + t_{13}) = P_2/P_1 = 50\%$ are expected within the framework of nonlocal thermal conduction. If CNTs are perfect ballistic thermal conductors, $t_{12}/(t_{12} + t_{13})$ should be independent of L_i. However, we find that ballistic phonons gradually dissipate and converge to the results of diffusive transport as L_i increases, suggesting that diffusive thermal conduction dominates when $L_i > 150$ to 200 nm.

Nonlocal thermal conduction can also explain the dissimilar anisotropic phonon scatterings observed in the T junction and the cross junction. When welding the perpendicular CNT into the horizontal CNT for the T junction, the phonon modes are pinched, in a way similar to inserting a microwave waveguide into another one. Because the CNTs are identical, the transmission (t_{13}) for forward scattering remains larger than t_{12}. On the other hand, due to the presence of the two CNTs welded sideways, the phonon modes are further pinched down in the cross junction; t_{13} becomes smaller than t_{12} or t_{14}. For $L_i > 150$ to 200 nm, decoherence of phonons dominates and the effect of the waveguide no longer applies, resulting in $t_{12} = t_{13} = t_{14} = 0.33$. When simulating the T junction and cross junction, we have also exchanged the temperature settings and verify $t_{ij} = t_{ji}$, confirming that the deviation to diffusive results is not due to thermal rectification. All these results have given consistent support to our previous findings of the dominant diffusive thermal transport for CNTs with $L_i > 150$ to 200 nm.

VI. OUTPUT RESISTANCE FROM A NONIDEAL HEAT BATH

From Table I, we find that the normalized interfacial resistance (AR_c) also varies from one to another. The origin of the discrepancy could be due to the fact that AR_c might not be simply scaled as the presumed cross-sectional area $A = \pi D \delta$ of CNTs. However, even for CNTs of identical chirality, AR_c can vary from 0 to 0.3×10^{-9} m² K/W, as shown in Fig. 5(c) for (10,10) CNTs. The variation could be due to different potentials, thermostats, or boundary conditions employed by different research groups. Curiously, we have found that AR_c is nearly independent of m_T and ΔT (Figs. 3 and 4), and it does not display apparent scaling with the diameter of CNT [Fig. 5(c)]. We also note the equivalent interfacial thermal conductance ($1/AR_c$) generally lies in the range of 10 GW/m² K, which is higher than the highest measured value (4 GW/m² K, occurring between

Al/Cu interface). The result indicates that the R_c is not a physical phenomenon, but rather an artifact from the nonideal thermostat.

An ideal thermostat should absorb all energy transmitting into it. However, it has been known that common thermostats (such as the Nosé-Hoover thermostat used here) are far from ideal and low-frequency phonons usually bounce back from them. Because of the phonon reflection from heat baths, Li and McGaughey proposed an interesting idea that energy transport could be diffusive even though phonon transport is ballistic [39]. Unfortunately, because the idea is based on the transient dynamics, it is difficult to test its validity based on our results under steady state conditions. On the other hand, because the steady state condition has been employed for experimental measurements, the concept of phonon and energy transport should be indistinguishable and the disagreements between experimental data and EMD/NEMD results are unambiguous.

An ideal voltage source should have zero output impedance in an electronic circuit. Similarly, an ideal thermostat with controlled temperature should have zero output resistance in a thermal circuit. However, due to the lack of ergodicity [40], the presence of temperature oscillations [41] and ill-defined temperatures in nonequilibrium processes [42,43], the commonly used thermostats (such as Nosé-Hoover thermostat used here) are known to be far from ideal. So it is not surprising that these thermostats always give nonzero output resistance when employing NEMD simulations. Curiously, because no other temperature jumps are observed in CNTs after excluding the apparent boundary effect shown in Fig. 2(b), the R_c found in the R_{total} vs L relations could happen inside the thermostats and function like the internal thermal resistance of a practical temperature source.

Similar to our daily experience of using a practical voltage source, the presence of finite output resistance in a thermostat would not be a problem in NEMD simulations once we are aware of the effect. In electronics, the nonzero output impedance of a voltage source reminds us to be cautious when measuring a highly conducting sample. Likewise, one should be alerted when employing a nonideal thermostat to simulate thermal transport properties of good thermal conductors like CNTs. Thus the presence of the unwanted R_c is not a serious problem. However, because both EMD and NEMD give consistent diffusive transport in CNTs, the inconsistency between MD and experimental results still cannot be resolved even if R_c is removed.

It should be noted that similar problems are also found in employing EMD and NEMD to simulate Si [44]. Dong *et al.* have found inconsistencies between EMD and NEMD and tried to resolve them by introducing an upper limit of the correlation time (t) in the Green-Kubo formula to be associated with the system length (L_x) and a free parameter v_g, using $L_x = v_g t$ [44]. Although they have claimed to observe a mean free path ∼300 nm in Si, we have instead found purely diffusive transport with finite R_c after replotting their data into AR_{total} vs L. The latter result still gives consistencies between EMD and NEMD even without introducing a fitting parameter. Because bulk Si with clean surfaces is experimentally known to exhibit mean free path at least longer than 1 μm [45], the disagreement suggests that the problems originate not only

from the thermostats employed but also from the empirical atomic potential of Si.

VII. DISCUSSIONS AND SUMMARY

These discussions certainly raise concerns on the validity of applying EMD or NEMD simulations to unravel thermal transport of CNTs. We note that the presence of R_c's has been pointed out in simulating 1D models [7]. The unwanted effect has been regarded as a finite size effect since then and α's can be obtained only from much larger systems [46,47]. Here, we find the unwanted R_c's of NEMD simulations on CNTs have also misled previous interpretations and should be removed. Moreover, although most EMD and NEMD simulations consistently yield diffusive thermal transport for $L > 200$ nm, the disagreements between the results and experimental data are especially disturbing. Because EMD and NEMD simulations apparently underestimate the ballistic thermal conduction observed in CNTs, it is likely the atomic potential overestimates the anharmonicity of the real potential of carbon sp^2 bonds, rendering the simulated temperature much higher than the experimental temperature (usually 300 K). If a lower temperature is employed in EMD and NEMD simulations, one might be able to observe non-Fourier thermal conduction at longer L's. Such a temperature correction has become commonplace in modeling water, and it is not surprising that similar corrections are needed for the empirical potentials used in MD simulations, too. Note that, however, the temperature correction is opposite to what "quantum correction" in MD would do, in which Bose-Einstein statistics is imposed to make the simulated temperature higher. Size effects on temperature, even for classical systems, could be another critical issue for simulating CNTs as well. Finally, the nonlinear effect associated with ΔT suggests that investigating non-Fourier thermal conduction in CNTs is not a trivial task. The long-time tails of phonon relaxation observed in 1D models could have been ignored during the simulation [3,4].

EMD or NEMD simulations have relied on either enforced thermal equilibrium or steady state to extract the nominal thermal conductivity, and NEMD has further constraints from the nonideal thermostat that gives rise to R_c mentioned above. Thus, how to make EMD/NEMD to reach agreements with Boltzmann transport models or experimental results could be a subtle issue. EMD and NEMD are not perfect approaches to evaluate thermal transport behaviors of CNTs, but they are nevertheless convenient to set up. They produce good guidelines for material designs when other approaches are not available, and they still give qualitative understandings on thermal transport behaviors of materials. However, it is important to recognize their limitations before extending them for practical uses. Our result now advocates cautious introspection on the fundamental limitations of MD simulations.

[1] S. Volz *et al.*, Eur. Phys. J. B **89**, 15 (2016).

[2] S. Lepri, *Thermal Transport in Low Dimensions: From Statistical Physics to Nanoscale Heat Transfer* (Springer, Berlin, Heidelberg, 2016).

[3] S. Lepri, R. Livi, and A. Politi, Phys. Rev. Lett. **78**, 1896 (1997).

[4] A. Dhar, Adv. Phys. **57**, 457 (2008).

[5] A. Dhar, Phys. Rev. Lett. **86**, 5882 (2001).

[6] B. W. Li, H. Zhao, and B. B. Hu, Phys. Rev. Lett. **86**, 63 (2001).

[7] K. Aoki and D. Kusnezov, Phys. Rev. Lett. **86**, 4029 (2001).

[8] G. R. Lee-Dadswell, E. Turner, J. Ettinger, and M. Moy, Phys. Rev. E **82**, 061118 (2010).

[9] Y. Y. Li, S. Liu, N. B. Li, P. Hanggi, and B. W. Li, New J. Phys. **17**, 043064 (2015).

[10] S. Maruyama, Physica B **323**, 193 (2002).

[11] S. Maruyama, Microscale Thermophys. Eng. **7**, 41 (2003).

[12] J. F. Moreland, J. B. Freund, and G. Chen, Microscale Thermophys. Eng. **8**, 61 (2004).

[13] C. W. Padgett and D. W. Brenner, Nano Lett. **4**, 1051 (2004).

[14] Z. H. Yao, J. S. Wang, B. W. Li, and G. R. Liu, Phys. Rev. B **71**, 085417 (2005).

[15] G. Zhang and B. W. Li, J. Chem. Phys. **123**, 114714 (2005).

[16] D. Donadio and G. Galli, Phys. Rev. Lett. **99**, 255502 (2007).

[17] J. R. Lukes and H. L. Zhong, J. Heat Transfer **129**, 705 (2007).

[18] K. D. Bi, Y. F. Chen, M. H. Chen, and Y. J. Wang, Solid State Commun. **150**, 1321 (2010).

[19] J. Shiomi and S. Maruyama, Int. J. Thermophys. **31**, 1945 (2010).

[20] J. A. Thomas, R. M. Iutzi, and A. J. H. McGaughey, Phys. Rev. B **81**, 045413 (2010).

[21] C. Sevik, H. Sevincli, G. Cuniberti, and T. Cagin, Nano Lett. **11**, 4971 (2011).

[22] K. Sääskilahti, J. Oksanen, S. Volz, and J. Tulkki, Phys. Rev. B **91**, 115426 (2015).

[23] N. Mingo and D. A. Broido, Nano Lett. **5**, 1221 (2005).

[24] L. Lindsay, D. A. Broido, and N. Mingo, Phys. Rev. B **80**, 125407 (2009).

[25] H. Y. Chiu, V. V. Deshpande, H. W. C. Postma, C. N. Lau, C. Miko, C. L. Forro, and M. Bockrath, Phys. Rev. Lett. **95**, 226101 (2005).

[26] C. W. Chang, D. Okawa, H. Garcia, A. Majumdar, and A. Zettl, Phys. Rev. Lett. **101**, 075903 (2008).

[27] J. H. Liu, T. Y. Li, Y. D. Hu, and X. Zhang, Nanoscale **9**, 1496 (2017).

[28] V. Lee, C. H. Wu, Z. X. Lou, W. L. Lee, and C. W. Chang, Phys. Rev. Lett. **118**, 135901 (2017).

[29] B. W. Huang, T. K. Hsiao, K. H. Lin, D. W. Chiou, and C. W. Chang, AIP Adv. **5**, 053202 (2015).

[30] M. Terrones, F. Banhart, N. Grobert, J.-C. Charlier, H. Terrones, and P. M. Ajayan, Phys. Rev. Lett. **89**, 075505 (2002).

[31] R. X. Su and X. Zhang, Appl. Therm. Eng. **144**, 488 (2018).

[32] J. Chen, G. Zhang, and B. W. Li, Nanoscale **5**, 532 (2013).

[33] L. F. C. Pereira and D. Donadio, Phys. Rev. B **87**, 125424 (2013).

[34] W. J. Evans, L. Hu, and P. Keblinski, Appl. Phys. Lett. **96**, 203112 (2010).

[35] M. Büttiker, Phys. Rev. Lett. **57**, 1761 (1986).

[36] M. Buttiker, Phys. Rev. B **38**, 9375 (1988).

[37] G. D. Mahan and F. Claro, Phys. Rev. B **38**, 1963 (1988).

[38] G. Chen, J. Heat Transfer **118**, 539 (1996).

[39] D. Y. Li and A. J. H. McGaughey, Nanoscale Microscale Thermophys. Eng. **19**, 166 (2015).

[40] P. K. Patra and B. Bhattacharya, Phys. Rev. E **90**, 043304 (2014).

[41] A. Guy and A. Bowling, J. Comput. Nonlinear Dyn. **12**, 031019 (2017).

[42] P. K. Patra and R. C. Batra, Phys. Rev. E **95**, 013302 (2017).

[43] P. K. Patra and B. Bhattacharya, J. Chem. Phys. **140**, 064106 (2014).

[44] H. K. Dong, Z. Y. Fan, L. B. Shi, A. Harju, and T. Ala-Nissila, Phys. Rev. B **97**, 094305 (2018).

[45] R. Anufriev, S. Gluchko, S. Volz, and M. Nomura, ACS Nano **12**, 11928 (2018).

[46] K. Saito and A. Dhar, Phys. Rev. Lett. **104**, 040601 (2010).

[47] L. Wang, D. H. He, and B. B. Hu, Phys. Rev. Lett. **105**, 160601 (2010).